Atmos. Chem. Phys. Discuss., 15, 13347–13393, 2015
www.atmos-chem-phys-discuss.net/15/13347/2015/
doi:10.5194/acpd-15-13347-2015

Atmospheric Chemistry and Physics Discussions

Composition, size distribution, optical properties and radiative effects of re-suspended local mineral dust of Rome area by individual-particle microanalysis and radiative transfer modelling

A. Pietrodangelo, R. Salzano, C. Bassani, S. Pareti, and C. Perrino

Institute of Atmospheric Pollution Research, National Research Council, Italy

Received: 1 April 2015 – Accepted: 13 April 2015 – Published: 7 May 2015

Correspondence to: A. Pietrodangelo (pietrodangelo@iia.cnr.it)

Published by Copernicus Publications on behalf of the European Geosciences Union.

Abstract

New information on the PM_{10} mineral dust from site-specific (Rome area, Latium) outcropped rocks, and on the microphysics, optical properties and radiative effects of mineral dust at local level were gained in this work. A multi-disciplinary approach was used, based on individual-particle scanning electron microscopy with X-ray energy-dispersive microanalysis (SEM XEDS), X-ray diffraction (XRD) analysis of dust, size distribution of mineral particles, and radiative transfer modelling (RTM).The mineral composition of Rome lithogenic PM_{10} varies between an end-member dominated by silicate minerals and one exclusively composed of calcite.

The first is obtained from volcanic lithotypes, the second from travertine or limestones; lithogenic PM_{10} with intermediate composition derives mainly from siliciclastic rocks or marlstones of Rome area. Size and mineral species of PM_{10} particles of silicate-dominated dust types are tuned mainly by weathering and, to lesser extent, by debris formation or crystallization; chemical precipitation of $CaCO_3$ plays a major role in calcite-dominated types.

These differences are evidenced by the diversity of volume distributions, within either dust types, or mineral species. Further differences are observed between volume distributions of calcite from travertine (natural source) and from road dust (anthropic source), specifically on the width, shape and enrichment of the fine fraction (unimodal at 5 µm a.d. for travertine, bimodal at 3.8 and 1.8 µm a.d. for road dust). Log-normal probability density functions of volcanics and travertine dusts affect differently the single scattering albedo (SSA) and the asymmetry parameter (g) in the VISible and Near Infrared (NIR) regions, depending also on the absorbing/non-absorbing character of volcanics and travertine, respectively.

The downward component of the BOA solar irradiance simulated by RTM for a volcanics-rich or travertine-rich atmosphere shows that volcanics contribution to the solar irradiance differs significantly from that of travertine in the NIR region, while similar contributions are modelled in the VIS.

ACPD
15, 13347–13393, 2015

1 Introduction

Airborne geological dust from topsoil and surface rocks represents a critical contribution to the total mass, composition, microphysical and optical properties of the atmospheric aerosol. The occurrence of lithogenic dust in the atmosphere implies that significant amounts of biological debris, complex organic molecules (i.e. humic-like substances), water and mineral particles may enter the composition of the airborne particulate matter (PM) (Hsu and Divita, 2009; Simon et al., 2010). Crustal particles commonly constitute the major mass fraction of the re-suspended lithogenic materials and influence significantly both the PM mass concentration at ground (Perrino et al., 2009; Viana et al., 2014) and the mineral composition. The latter varies mostly depending both on the rock types outcropping in the source region (Dürr et al., 2005; Journet et al., 2014) and, consequently, on the crystallization, sedimentation and weathering processes tuning the particle size and shape (Claquin et al., 1999). This has been observed for mineral dust of African desert regions (Caquineau et al., 2002; Evans et al., 2004; Stuut et al., 2009; Scheuvens et al., 2013; Formenti et al., 2014) and of arid areas in other regions (Kim et al., 2006; Jeong, 2008; Moreno et al., 2009; Agnihotri et al., 2013; Rashki et al., 2013). Either microphysical (size distribution and complex refractive index) and optical properties of airborne lithogenic dust vary as a consequence of the mineralogical composition (Sokolik and Toon, 1999; Reid et al., 2003; Hansell et al., 2011; Wagner et al., 2012; Di Biagio et al., 2014; Mahowald et al., 2014; Smith and Grainger, 2014). When at a certain site intrusions of lithogenic dust at ground occur, like desert dust, the overall properties of the PM may be altered, compared to periods when this contribution is negligible (Meloni et al., 2006; Choobari et al., 2014). This also affects the impact of airborne aerosol on the energy balance of the Earth–solar system. Airborne lithogenic dust plays a role both in the direct mechanisms (light scattering and absorption) and in the indirect mechanisms (warming or cooling of the atmosphere) which tune the Earth's radiative budget (Sokolik et al., 2001; Choobari et al., 2014). While indirect effects depend on the heterogeneous chemistry occur-

ACPD
15, 13347–13393, 2015

ring at particles surface (Levin et al., 1996; Buseck and Pósfai, 1999; Sokolik et al., 2001; Krueger at al., 2004; Kandler et al., 2007), the light scattering and absorption are mostly controlled by the mineralogical composition, shape features and microphysical properties of geological particles (D'Almeida, 1987; Kalashnikova and Sokolik, 2002 and 2004; Kokhanovsky, 2008; Hansell et al., 2011).

Most studies facing this issue relate to desert dust from Sahara and Sahel regions (Kandler et al., 2007, 2009; Müller et al., 2009; Papayannis et al., 2012; Wagner et al., 2012; Di Biagio et al., 2014). Nevertheless, knowledge gaps still exist on this issue (Rodríguez et al., 2012), due to the site-related large variability of dust mineralogical features (elemental and mineral composition, crystalline structure, shape, microphysical and optical properties).

Also, only few of the published studies characterize the re-suspended geological dust of non-African regions (Falkovich et al., 2001; Peng and Effler, 2007; Rocha-Lima et al., 2014). Large areas of Italy, especially those closer to the Mediterranean Basin, are affected by dryness, heavy anthropic impact (urbanization, farming, quarry activities, etc.), erosion and poor vegetation cover, leading to increased desertification risk. The National Atlas of areas under risk of desertification of Italy reports, for instance, that the yearly average of dry soil days in the region of Latium ranges 64–110 (Costantini et al., 2007 and 2009). In Fig. S1 in the Supplement this is showed for the area of study of this work; the highest number of dry soil days (86–110) is found in the northern zone of the study area (Geoportale Nazionale, 2011). Latium is also affected by high rain aggressiveness, within the scale of FFAO index, and is characterised by a large surface where poorly-developed soils and debris deposits are present, which are easily affected by massive erosion.

Considering also the high anthropic impact on the Latium territory, it has to be expected that the re-suspension of mineral dust from local lithological domains is non-negligible in this region. Within this picture, main goals of this work were: to study the relationships between the local outcropped rocks (or topsoil) and the airborne dust particles sourced from these rocks, and to gain knowledge about the influence of local min-

ACPD
15, 13347–13393, 2015

eral dust on the airborne PM in Rome, in terms of microphysical and optical properties, and by modelling the downward radiative flux at BOA (Bottom Of Atmosphere) relating to the presence of local mineral dust. In a previous study, we determined elemental source profiles of the PM_{10} fraction of local mineral dust (Pietrodangelo et al., 2013). In this work, the PM_{10} fraction of the same samples was characterized with respect to the above goals. To investigate relationships among these different aspects, a multi-faceted analysis was performed, on the basis of the following approaches: individual-particle scanning electron microscopy combined with X-ray energy-dispersive microanalysis (SEM XEDS), bulk mineralogical analysis by X-ray diffraction (XRD), parameterization of the size distribution to log-normal function, and radiative transfer modelling (RTM). Results from experimental and modelling analysis are discussed for their consistency with both the lithological nature of major local dust sources and the microphysical properties of the mineral dust samples.

2 Approach and methodology

2.1 Study area, dust collection and sample treatment

Mineral dust was collected from topsoil and debris of rural areas surrounding the city of Rome within a perimeter of 50 km radius. Collection areas of about 4 km^2 were selected on the basis of criteria established after geological analysis of the Latium region, within main local geodynamics domains, namely: the volcanic complexes, the marine (limestones, marlstones and sandstones) deposits, the siliciclastic series (mainly flysch) and the quaternary deposits (mainly travertines). Furthermore, paved road dust was collected by brushing the surface of different roads within the volcanic and the travertine domains. PM_{10} dust was laboratory re-suspended from the bulk rocks samples, and from road dust, by a re-suspension chamber, and collected by low-volume sampling on polycarbonate membranes for SEM XEDS microanalysis. The whole geological siting criteria, dust sampling strategy, laboratory treatment details and elemental profiles of

ACPD
15, 13347–13393, 2015

the re-suspended dust types, are fully described in Pietrodangelo et al. (2013). In that paper we discussed how, under the perspective of mineral composition, the volcanics (silicate-dominated rocks) and the travertine (calcite-dominated rocks) can be considered as reference compositional end-members of the overall outcropping lithotypes in the Latium region (Cosentino et al., 2009), while the sedimentary domains (marine deposits and siliciclastic series) represent intermediate compositional terms. Therefore, for the scopes of this work the complete procedure of dust characterization (elemental and mineral composition, size distribution, optical properties and radiative downward flux) described in the following sections was applied only to the volcanics and travertine dust.

2.2 Individual particle microanalysis

An environmental scanning electron microscope Philips XL30 ESEM (FEI Company, tungsten filament) equipped with an energy dispersive spectrometer for X-ray microanalysis (EDAX/AMETEK Inc., USA) was used for individual particle characterisation of the PM_{10} dust. A small portion of sample (about 8 % of total filter area) was cut in the centre of polycarbonate membranes, fixed to aluminium stubs by self-adhesive carbon discs (TAAB, 12 mm diam.) and coated with an ultra-thin carbon layer by a vacuum evaporator (108 Carbon A, Cressington, Scientific Instruments Ltd., UK). SEM XEDS acquisitions were performed under high vacuum (10^{-6} hPa) at 20 keV accelerating voltage, allowing the K-line excitation of elements with atomic number $Z \leq 27$ (Co, Kα 6.923 keV). Micrographs were acquired by secondary electron detector (SED) at magnification, working distance (WD), tilt angle and spot size conditions properly adjusted on a case-sensitive scale to optimize image resolution. The microanalysis was performed at WD 10 mm (take-off angle 35° relative to the specimen plane) on field areas of 1290–5200 µm^2 (magnitude × 6000–3000) spread on the overall specimen surface; between 700 and 1000 particles were analysed per sample.

The Particle/phase analysis v.3.3 package (EDAX Inc., 2000) was used for the automated individual particle microanalysis; threshold of the digitalised object area to be

ACPD
15, 13347–13393, 2015

analysed was set at 80 %. Since a great number of individual particles was analysed, short live times (20–30 s) were imposed to XEDS spectra acquisition. Each field of microanalysis was manually selected prior to launch the automated scanning of particles. This choice allows a field-specific tuning of the grey scale, in order to minimize brightness *artifacts* in the automated identification of particles. Amplification time and spot size were adjusted to ensure dead time around 30 % and total counts rate above 500 cps. In addition to automated microanalysis, manual acquisitions were carried out, either on field areas and on individual particles, by using the EDAX control v. 3.3 package (EDAX Inc., 2000). About 20 to 30 field areas were selected from the different dust samples to perform manual acquisitions. These have been run in triplicate on each field (live time 10–20 s), to assess the repeatability of the microanalysis.

Further, XEDS spectra acquired from areas included in these fields were quantified by the conventional standard-based quantification procedure of bulk materials, to assess consistency with results previously obtained by ED-XRF analysis (Pietrodangelo et al., 2013).

Manual microanalysis of 15 to 30 individual particles per-sample was also performed, and high resolution micrographs of these particles were stored. Magnification above 6000× and longer live times (30–60 s) were employed, so that resulting XEDS spectra have total counts rate ranging 5000–10 000 cps. These data were used both to assess the accuracy of microanalysis with respect to different mineral particles (Table 1), and to perform the quantification of individual-particle XEDS spectra by an internal standard approach, as further discussed in Sect. 2.3 and 3.1.1.

2.3 Quantification of individual particle XEDS spectra and apportionment to mineral classes

A large data set of XEDS spectra and size (Feret diameters, area, aspect ratio, roundness) of individual dust particles was stored. To apportion dust particles into main mineral classes of our dust samples, an ad-hoc procedure has been adopted.

ACPD
15, 13347–13393, 2015

First, the bulk mineral composition of dust samples was determined by X-ray diffraction (XRD), to identify major minerals in the dust samples. Then, XEDS spectra of individual particles were semi-quantified and matched to spectra and to elemental composition of reference pure minerals expected after XRD analysis. Results of matching were used to apportion individual particles into main mineral classes. Details are described below.

The mineralogical characterization of dust samples has been carried out on the 50 µm sieved dust fraction, by an automatic diffractometer Scintag X1, equipped with a Si(Li) detector using a Cu Kα, under the following conditions: Ni-filtered radiation, step-scan modality (2° step = 0.02°), acquisition time of 10 s, operating at 45 kV and 40 mA. Quantification of minerals has been obtained according to procedures defined by Moore and Reynolds (1997).

A random orientation of particles was obtained by pressing 0.5 g of the 50 µm sieved materials with 5 atm for 10 s. Quantitative determinations were obtained by using appropriated standards and elaborating spectra as indicated in Giampaolo and Lo Mastro (2000). From XRD results and on the basis of previous geological analysis of the area, mineral species to which individual dust particles have to be apportioned were identified.

Apportionment of individual dust particles analyzed by SEM XEDS can be carried out by matching XEDS spectra of particles to those of pure minerals. However, XEDS spectra of some minerals can be not available; in this case, apportionment can be performed by matching the quantified elemental composition of particles with that of pure minerals.

Therefore, prior to the apportionment procedure, particle elemental composition had to be quantified. When quantification of individual particle XEDS spectra is concerned, the use of conventional methods for bulk and thin polished materials (Castaing, 1951) imposes some critical limitations, and proper adjustments and assumptions for the theoretical treatment of X-ray generation and losses in the particulate matrix are needed (Armstrong and Buseck, 1975; Van Dyck et al., 1984; Chožl et al., 2005, 2007).

ACPD
15, 13347–13393, 2015

In addition to bulk matrix effects, the particle size and shape play a major role in the mass, absorption and fluorescence effects of particulate matrices (Fletcher et al., 2011). In this study, the mass effect (induced by particle thickness lower than the spot size of primary electron beam) was considered negligible. Dust particles selected for quantification, indeed, show an equivalent projected area diameter (assumed as particle thickness according to Kandler et al., 2007) above 2 µm, that is far larger than the spot size used (0.3–0.4 µm average). However, energy losses due to particle absorption and fluorescence effects cannot be neglected. Among methods described in literature to quantify environmental particles by XEDS microanalysis (Fletcher et al., 2011), the particle standard approach was adopted in this work. In particular, an internal standard was used; by this choice, particle matrix effects are included in the quantification process, and the conventional standard-based quantification method still can be used (Castaing's first approximation corrected for bulk matrix effects by the ZAF algorithm).

First, high-counts spectra of particles analyzed manually in the dust sample matrix (as described in Sect. 2.2) were quantified by the standard-based routine available from EDAX control v. 3.3 package (Newbury and Ritchie, 2013); to this aim, the pure minerals available from EDAX Library have been used as standards. Long acquisition time and high counts of these spectra are expected to minimize the statistical error of quantification (Goldstein et al., 1986). From the EDAX quantification routine, the element Z (atomic number), A (absorption) and F (fluorescence) correction factors, related to the influence of the particulate matrix on X-ray losses of individual particles, are obtained for each analyzed particle of a sample.

Element ZAF mean values, differentiated by dust sample, were then obtained by averaging, within each sample, ZAF values of all analyzed particles. Finally, the sample-specific mean ZAF values were used in the quantification of particle spectra obtained by automated microanalysis. The conventional standard-based ZAF-corrected Castaing's method was used also in this case; however, the standard element concentration and ZAF were those of the manually-analyzed particles. By this procedure, in-

ACPD
15, 13347–13393, 2015

deed, manually analyzed particles could be assumed as internal particle standard, on a sample-specific base. The reliability of quantification of manually analyzed particles, by Castaing's first approximation approach, was evaluated in terms of accuracy with respect to mineral standards available from the EDAX Library. Details and results are discussed in Sect. 3.1.1.

Particles showing total sum of element percent weight (%wt) below 50 (including oxygen estimated by element oxides) were not further considered in the rest of the study.

Reference XEDS spectra and elemental composition of pure minerals, to be used for particle apportionment, were obtained either from the EDAX Library (biotite, clorite, calcite, diopside, kaersutite, olivine, plagioclase and quartz) or by the RRUFF project (Downs, 2006) and GEOROC (Sarbas and Nohl, 2008) open-source databases, available on the web. Minerals collected from Central Italy were preferred where possible.

Spectral matching was performed by the chi-square test for spectral goodness of fit included in the Library matching v.3.3 application (EDAX Inc., 2000). In cases where spectral matching couldn't be performed, apportionment of particles to mineral species was obtained on the basis of the best fit of the dust particle %wt element composition vs. the composition of pure minerals, by single linear regression analysis (SLR). The reliability of the internal standard approach has been evaluated by assessing the consistency of the apportionment to mineral species (which directly depends on results of quantification by internal standard approach) with XRD analysis.

Apportioned mineral particles of the volcanic and travertine dusts were then used to investigate the microphysical, optical and radiative properties of the PM_{10} lithogenic dust of Rome.

2.4 Size distribution

Physical size of particles was assumed as the diameter of the equivalent cross sectional area (ESD) (Reid et al., 2003; Kandler et al., 2007; Chožl et al., 2007) measured by SEM. Then, mineral density was assigned to apportioned particles; volume, mass

ACPD
15, 13347–13393, 2015

and aerodynamic diameter were consequently calculated (Kulkarni et al., 2011). On this basis, the volume size distributions of most representative mineral species observed in this study (kaolinite, quartz, feldspar and calcite) have been built.

2.4.1 Probability density function

The probability density functions (PDF) of the volcanics and travertine PM_{10} dust were estimated by fitting the frequency distribution of particle size to log-normal curve. Frequency distributions of volcanics and travertine were built on the basis of the size bins of the GRIMM 1.108 optical particle counter (OPC). The fitting procedure was developed using the R-Project programming environment (R Core Team, 2013) and the routine was implemented by a general-purpose optimization based on Nelder–Mead algorithm (Nash, 1990).

The procedure attended to minimise the deviation between observed distribution and log-normal model. This is expressed by the equation (Davies, 1974):

$$\frac{dN(r)}{d\log r} = \frac{N}{\sqrt{2\pi}\log\sigma}\exp\left(\frac{-1}{2}\left(\frac{\log r - \log r_m}{\log\sigma}\right)^2\right) \quad (1)$$

where N is the number of particles, r_m is the mean radius of particles, and σ is the standard deviation (SD) of r. Quality assurance of the fitted models was evaluated considering the "chi squared" index (χ^2) in order to estimate the level of acceptance (Wilks, 2006).

This index is proportional to the sum of squares of the difference between each data point and the corresponding computed value. The level of acceptance was defined using the χ^2 distribution tables.

2.5 Radiative transfer modelling

An atmospheric radiative transfer code was employed, generally used in the remote sensing, to retrieve the optical and radiative dust properties. The 6SV (Second Simula-

ACPD
15, 13347–13393, 2015

tion of a Satellite Signal in the Solar Spectrum – Vector) (Vermote et al., 2006; Kotchenova et al., 2008) is the new-generation open-source atmospheric radiative transfer model 6S (Second Simulation of a Satellite Signal in the Solar Spectrum) (Vermote et al., 1997). This code is able to retrieve optical properties of the aerosol and to model the atmospheric radiative field by using the aerosol microphysical properties, under the hypothesis of spherical and dry particles. Microphysical properties of aerosol required for the modeling are the size distribution and refractive index. Size distributions targeted to the type of aerosol can be introduced as input in the 6SV code. To this aim, frequency distributions of particle size of the volcanics and travertine PM_{10} were processed for curve-fitting, as described in Sect. 2.4.1. Log-normal curve parameters r and σ of the two dust types were thus used as inputs in the 6SV code.

The real and imaginary parts of the refractive index were assumed from literature.

The refractive index of the "water-insoluble" aerosol component reported in Kokhanovsky (2008) was associated to the volcanics dust of Rome area. This component is indeed defined as mainly dust, rich in water-insoluble minerals e.g. silicates, and is reported in literature in the spectral domain considered by the 6SV code. In the case of travertine dust, the calcite refractive index data reported by Ghosh (1999) were used.

The 6SV code retrieves aerosol optical properties by the Mie Theory and simulates, afterword, the radiative modeling by solving the radiative transfer equation (RTE) in the solar spectral domain. By this way, the propagation of solar radiation in the Atmosphere/Earth coupled system can be completely described.

Runs of 6SV code were performed on a setting of parameters related to the site-specific meteorological and atmospheric conditions, and to the aerosol loading and microphysical properties. Concerning meteorological parameters, the profiles of temperature, pressure and humidity were assumed by the *1976 U.S. Standard* Atmosphere included in the 6SV code.

Atmospheric conditions were established in order to model the radiative field under daily *maximum Sun* elevation in Rome area; a spring day, 12 May, at midday was thus

ACPD
15, 13347–13393, 2015

selected. Columnar contents of water vapor and of ozone were fixed to 1.32 cm and 0.283 Db, respectively. To describe the aerosol loading, the aerosol optical thickness at 550 nm, τ_{550} (Vermote et al., 1997; Kaufmann et al., 1997; Bassani et al., 2010, 2012) is commonly considered. The atmospheric profile of the aerosol is assumed to be exponential with a scale height of 2 km (Vermote et al., 1997). In this study, however, an higher value of aerosol optical thickness, $\tau_{550} = 0.7$, was chosen, in order to allow describing a scenario where the local geological dust loading has a major role when the radiative field in the atmosphere/earth coupled system is simulated.

Among optical properties, the single-scattering albedo and the asymmetry parameter were chosen, as they are crucial to perform analysis of the aerosol contribution on the radiative field (Dubovik et al., 2002; Kassianov et al., 2007).

Concerning the simulation of the radiative quantities, the downward irradiance was modelled, to the aim of performing a preliminary investigation on the radiative impact of the different dust types in the Earth–atmosphere coupled system. The volcanics and travertine PM_{10} local dust are expected to show significantly distinct microphysical properties, due to their compositional differences. Radiative modelling has been performed thus on the assumption of an atmosphere where the only aerosol component is volcanics or travertine dust, separately.

Results are showed in Sect. 3.5.2 and 3.5.3.

3 Results and discussion

Results of individual-particle XEDS spectra quantification and classification into mineral species are reported in Sect. 3.1–3.3. In particular, the discussion concerns the reliability of microanalysis and of high-counts spectra quantification (Sect. 3.1), a principal component analysis (PCA) of particles elemental composition (Sect. 3.2), the apportionment into mineral classes and the reliability of quantification by the internal standard approach used in this work (Sect. 3.3). In Sect. 3.4 volume size distributions are discussed, and differences between calcite from a lithogenic source (travertine dust)

ACPD
15, 13347–13393, 2015

and from an anthropogenic material (paved road dust) are also evidenced. Finally, in Sect. 3.5 the microphysical and optical properties, and the downward component of radiative flux at BOA (Bottom Of Atmosphere) in a volcanics-rich or travertine-rich atmosphere are discussed, with respect to the features of Rome area.

3.1 Reliability of XEDS microanalysis and quantification

In Table 1 (upper part) the repeatability of XEDS microanalysis and consistency with the ED-XRF analysis are reported. Repeatability was evaluated by triple field acquisitions (number of fields: 20–30) from each PM_{10} dust sample. Large fluctuations around mean (% relative SD) are observed for light (Na and Mg principally) and trace (Mn and Ti) elements. Consistency with previously obtained elemental profiles of the PM_{10} fraction (Pietrodangelo et al., 2013) by ED-XRF, was assessed by matching to the latter the percent weight element composition of micro-areas of the dust samples obtained by XEDS field microanalysis. Results indicate that the microanalysis is less reliable for Na, Mn and for Si and Mg in the siliciclastics sample, while in all other cases it shows a good agreement with ED-XRF bulk analysis.

Quantification results of manually acquired XEDS individual particle spectra are also reported in Table 1 (lower part), for kaersutite, quartz and calcite. Quartz and calcite represent the compositional end-members of mineral species observed in the dust samples of this work. Kaersutite particles were frequently observed during manual acquisitions. As this silicate mineral include in its composition non-negligible presence (above 4 %wt) of the principal crustal elements (Si, Al, Na, Mg, K, Ca and Fe), it has been assumed as reference term for the microanalysis of silicate particles. XEDS spectra of kaersutite, calcite and quartz particles are showed in Figs. S3–S5 in the Supplement, respectively.

The element composition is reported in terms of element mass in the electron interaction volume at 20 KeV; the latter was estimated for quartz, kaersutite and calcite according to Potts (1992). Uncertainties of quantification are large for K, Na, Mn and Ti, as expected due to the poor sensitivity of XEDS microanalysis to light and/or

ACPD
15, 13347–13393, 2015

trace elements, whereas they range 1–10 % relative error for other elements. Element uncertainties reported in Table 1 were estimated following the approach by Ziebold (1967), after assigning the proper peak-to-background ratio to each element in each mineral particle. The compositional differences of individual particles of quartz, calcite and kaersutite, with respect to related bulk mineral standards, are also reported in Table 1 (last rows) in terms of absolute percent differences between the element %wt in the standard mineral and that in the mineral particle.

As expected from the uncertainties, major compositional differences with respect to mineral standards are observed in Na, Mn and Ti quantification of kaersutite; also the quantification of Ca differs largely from the mineral standard, both in kaersutite and in calcite particles.

3.2 Elemental composition of individual dust particles

Particles included in the data set are individually codified with respect to the respective dust source, so that they are traceable in the statistical processing of data. Comparing information extracted from a multivariate statistical analysis of this data set, on the dust type to which each particle is ascribed, to same information certainly known from particle codification in the same data set, allows the evaluation of soundness of the elemental composition data and, consequently, of the quantification approach applied to particle XEDS spectra.

To this goal, a principal component analysis (PCA) of the elemental ratios commonly used to discriminate among different mineral classes (Al/Ca, Fe/Ca, K/Ca, Mg/Ca, Ti/Ca, Si/Al, Si/Fe, Ti/Fe and Ti/Mn) was performed. The XLSTAT 7.5 statistical package (Addinsoft) was used, with Varimax rotation and extraction of the latent factors; results are showed in Figs. 1 and 2. Three latent factors with eigenvalue higher than unity explain 76 % of the total variance of particle composition. The element/Ca ratios mainly contribute to the first factor (F1, eigenvalue 4.5), the Si/Al and Si/Fe ratios contribute to the second factor (F2, eigenvalue 1.8), while the Ti ratios are rep-

ACPD
15, 13347–13393, 2015

resented by the third factor (F3, eigenvalue 1.3). In Fig. 1, particle scores are reported in the F2 vs. F1 and in the F3 vs. F2 plots.

Particles described by the F1 are ascribed to volcanics and, in minor fraction, to siliciclastics dust. The latter are indeed described mainly by the F2. Finally, road dust and travertine particles are grouped by the F3. Marlstone particles were not included in the PCA and in the subsequent parts of the study, due to the smaller number of available data with respect to the other samples. To assess the soundness of the PCA solution, the relative Si and Ca abundance and the equivalent spherical volume (ESV) have been examined, within clusters identified by the F1, F2 and F3. In Fig. 2, the Si and Ca abundances of particles with factor score higher than unity on each of the three latent factors have been plotted with respect to the ESV.

Since the average mass fractions of Si and Ca, in SiO_2 and $CaCO_3$ respectively, are 0.47 and 0.4, the threshold of 0.4 can be used to discriminate qualitatively either between silica and silicates (for which Si abundance is expected roughly below 0.4), and similarly between calcite and other Ca-bearing particles. Median Si abundance of both volcanics and siliciclastics particles in F1 is 0.37–0.39 (Fig. 2a); also Ca abundance is similar in both particle groups (below 0.1). Median values of particle ESV are 3 μm^3 (volcanics) and 3.5 μm^3 (siliciclastic), although a very large variability was measured. Upon the above considerations on the Si mass fraction in SiO_2, a silicate nature of these particles might be supposed. Particles grouped by the F2 (Fig. 2b) are mainly siliciclastic and only a minor fraction is ascribed to volcanics. All these particles share both the Si and Ca abundances (0.6 and 0.1, respectively), and the median ESV (3–3.5 μm^3), the latter being comparable with the ESV of F1 particles. Si abundances far above 0.4 suggest that these are silica particles. It should be also noted that, as particles in F1 and F2 show similar ESV but different Si abundance, differences in the particle density can be supposed between these two groups. Finally, particles with the highest score in F3 (Fig. 2c) are mainly ascribed to road dust and travertine samples and show Ca abundances around 0.4, which can be related to $CaCO_3$.

ACPD
15, 13347–13393, 2015

The PCA solution found on the XEDS data set of particle elemental composition is thus coherent with the real mineralogical nature (silicate or calcite) of particles, indicating that the sample-targeted internal standard approach applied to the quantification of particle composition provided reliable results.

3.3 Mineralogy of samples and apportionment of individual particles

The mineralogical composition quantified by XRD analysis is reported in Table 2.

Main differences concern the increasing amount of calcite (volcanics < siliciclastic rocks < marlstones < travertine), the absence of inosilicates in siliciclastic rocks and travertine, the negligible amount of phyllosilicates in travertine and the considerable presence of quartz in siliciclastic rocks. All of these features are consistent with the geological processes involved in the formation of each rock type. Calcite is a geochemical marker of the sedimentary environment where rocks are formed and it is associated to the chemical precipitation of calcium carbonate. As a consequence of that, while its presence in volcanic rocks is negligible, in the marine deposits (marlstones) it is dominant and in the siliciclastic series it represents the second most abundant mineral component after phyllosilicates.

Moreover, it is the almost exclusive component of travertine, generated by the precipitation of $CaCO_3$ near the hot hydrothermal springs of the Tivoli basin (Pentecost, 2005; Faccenna et al., 2010). The silicate component of marlstones and siliciclastics dust suggests that weathering processes are mainly responsible of the PM_{10} fraction of these dust types. This is evident by the presence of both stable silicates (plagioclase and quartz), which in the sedimentary domains can be ascribed to debris phases, and phyllosilicates. The latter are dominant also in the mineralogical composition of the volcanics dust, indicating once more the importance of chemical weathering. As an example, in the volcanics PM_{10} the kaolinite has been frequently observed, evidencing the possible occurrence of the hydrolysis reaction of feldspars (Jackson et al., 2010). This process is well described by the association kaolinite–quartz, observed by SEM

ACPD
15, 13347–13393, 2015

XEDS microanalysis. In this case thus the quartz is not a crystallization-derived phase, but a weathering by-product.

Considering the results of the apportionment procedure (Sect. 2.3), mineral particles in the PM_{10} dust samples were mainly classified as: phyllosilicates (kaolinite, smectite and micas), representing more than half of the silicate (non-quartz) fraction of the totality of samples, tectosilicates (feldspar, chabazite, leucite and plagioclase) and inosilicates (clinopyroxene and amphibole), which contribute comparably to the rest of silicate fraction, quartz and calcite. About 65 % (percent abundance) of total phyllosilicates are found in the volcanics, being mainly kaolinite (observed in the volcanics only) and 60 % of total observed smectite. Micas are also frequently observed, mainly in the siliciclastics sample. Concerning tectosilicates, the overall contribution apportioned to the PM_{10} of each geological domain and of road dust has been found to be 47 % in the volcanics, 20 % in the siliciclastic rocks, 33 % in the road dust, while it appears negligible in the marlstones. Inosilicates were observed in similar amounts, and solely in the volcanics and in the road dust. About half of quartz particles identified in the totality of PM_{10} dust samples is apportioned to siliciclastic rocks, while volcanics, marlstone and road dust provide equally to the remaining fraction. Finally, within the non-travertine sedimentary rocks of this study, the marlstones provide the most important contribution of calcite particles in the PM_{10} fraction (ab. 35 %), while the contribution of siliciclastic rocks is around 8 %. Similar contributions than marlstones are also apportioned to road dust. These results, obtained by the apportionment procedure, are in good agreement with the mineralogical composition by XRD (Table 2).

To assess the reliability of apportionment, a mass closure approach was used.

The particulate mass fraction of each mineral group in the PM_{10} (sum of particles mass within a mineral group, per dust sample) was estimated from results of the apportionment after SEM XEDS microanalysis. Afterwards, the PM_{10} weight percent composition of the total silicate (including quartz) content and of the calcite content were calculated; these quantities were then compared to the corresponding quantity ob-

ACPD
15, 13347–13393, 2015

tained by XRD analysis of the 50 µm sieved fraction of each dust sample, as reported in Fig. 3.

Although the travertine was not analyzed by XRD, since it can be considered a pure calcite term (Pentecost, 2005), results of the mass apportionment by SEM XEDS have been reported for this sample too. In all dust samples (excluding the case of travertine), a good comparability with analytical results of mineral composition by XRD are observed for mass estimates obtained from the apportionment of individual particles. Besides indicating that the apportionment procedure produced reliable results, this also suggests that the silicate and calcite contents of the PM_{10} and of the 50 µm sieved fractions of dust are likely similar, as yet reported in literature (Rashki et al., 2013).

3.4 Connections between geochemical processes of rock sources and the PM_{10} fraction of minerals

The size distribution of re-suspended geological materials is influenced by two important contributions: the physical properties of particles (e.g. size and density), which affect the dust re-suspension and transport; and the geological features of the rock source, which determine the particle mineralogical identity. In this view, size distribution of the PM_{10} fraction has been discussed either for individual mineral species (quartz, kaolinite, feldspars and calcite), or for the overall local lithogenic dusts (volcanics, siliciclastic rocks and travertine); in the latter case the totality of mineral particles identified in each dust type was considered. In Sect. 3.4.1, size distributions of individual mineral species have been investigated with respect to the clay fraction according to Claquin et al. (1999), Nickovic et al. (2012), and Journet et al. (2014), while in Sect. 3.4.2 volume distributions (Formenti et al., 2014) of mineral species and of lithogenic dusts are discussed.

ACPD
15, 13347–13393, 2015

3.4.1 Clay fraction of minerals

In this part of the study the classified mineral particles were treated with respect to the geochemical processes which they can be related to, with the aim of relating the size distribution of each mineral species to the geochemical processes acting on the rocks to generate the PM_{10} fraction of that mineral species. Therefore particles are here named as: (1) phyllosilicates, including clay-minerals (kaolinite, illite, smectite and chlorite groups), and representing thus the contribution of weathering and pedogenesis to the re-suspension from outcropping rocks; (2) "other silicates", including phases such as plagioclase, K-feldspar, pyroxene and quartz, which can be considered as crystallization products in volcanics rocks, or debris phases in sedimentary rocks; (3) calcite, differentiated by lithogenic and road dust particles. The approach of Claquin et al. (1999) was adopted in choosing mineral species for which the mass percentage in the clay fraction (particle size $< 2\,\mu m$) was calculated, on the basis of the particle ESD. Mass percentages of mineral in the clay fraction of PM_{10} dust samples of this study were compared with those obtained by Journet et al. (2014) for the modelled global yearly average composition of airborne minerals. With respect to the latter (abbr. *gyac*), the mineral composition of the Rome local geological PM_{10} shows the following similarities, or discrepancies: (1) the amount of quartz in the clay fraction of the siliciclastic PM_{10} (20 %) and of the volcanics PM_{10} (8 %) is significantly higher compared to the *gyac* (4.9 %); (2) feldspars in the clay fraction of both the volcanics (4 %) and siliciclastic PM_{10} (2.5 %) are comparable to feldspars in the *gyac* (3.6 %); (3) kaolinite dominates the clay fraction of the volcanics PM_{10} (63 %) and it is negligible in the other PM_{10} dust types (ca. 2.5 %), while in the *gyac* it represents 24.1 % of total mass; (4) smectite in the Rome local geological PM_{10} ranges 3 to 10 %, that is lower compared to *gyac* (15.3 %).

Considering the distribution of particles in the clay and non-clay (ESD $> 2\,\mu m$) fractions of the mineral PM_{10} of Rome area, main differences are observed for the volcanics and the travertine types. In the volcanics PM_{10} the weathering by-products (quartz,

ACPD
15, 13347–13393, 2015

kaolinite and smectite) are comparably distributed in the two size fractions, indicating that weathering processes produce either small grain-sized crystals, and altered phases which grow on the surface of large crystals, resulting in larger particles. The crystallization phases produced in the volcanics PM_{10} (feldspars and pyroxene) are instead enriched in the non-clay size, as implied in the crystallization process.

Source-related differences between natural calcite from travertine and calcite from road dust were also evidenced. The clay/non-clay distributions of calcite in the PM_{10} of either the travertine dust and the road dust travertine-related, differ significantly from the clay/non-clay calcite distribution in the PM_{10} of road dust volcanics-related. While in the first case the calcite is comparably distributed in the clay/non-clay size, the mass percentage of this mineral in the road dust volcanics-related is higher in the clay size (80 %) than in the coarser size (60 %). Since the presence of calcite in the volcanics PM_{10} is negligible, calcite content in the PM_{10} road dust collected in the volcanics can only be ascribed to the asphalt contribution.

It is thus reasonable that this anthropogenic source enrichs the size fraction below 2 µm (ESD) of calcite, more than the coarser one. This effect is less evident, instead, in the road dust travertine-related, where the lithological influence of travertine rocks assumes a major role in the clay/non-clay distribution of calcite.

3.4.2 Volume size distribution of the PM_{10} fraction: minerals and lithogenic dust types

The volume size distributions of quartz, feldspars, kaolinite and calcite are reported in Fig. 4 vs. the aerodynamic diameter (a.d.); in this figure, particles have been grouped with respect to belonging to a given mineral species, without differentiating by geological domain. Figure 4a shows the distributions of kaolinite, quartz and feldspars, while in Fig. 4b distributions of calcite in the two different road dust types and in travertine are shown.

Volume distributions of the considered silicates are unimodal, with overlapping maxima around 5 µm. Main differences are in the peak width: weathering minerals, such as

ACPD
15, 13347–13393, 2015

kaolinite, show a broader curve, compared to minerals from crystallization phases, e.g. feldspars. This is coherent with the above described action of the weathering, of generating particles either in the clay-fraction, and in the coarser size, which contributes to broaden the size range.

Quartz shows an intermediate behaviour, due to different processes acting on quartz formation: weathering in the volcanics, crystallization in the siliciclastics.

The different nature of geochemical processes affects also volume distributions of the overall lithogenic dust types (Fig. 4c). Particularly, volcanics and siliciclastics dusts show broader distribution than travertine, due to the dominance of weathering, in the formation of lithogenic PM_{10} from volcanic and siliciclastic rocks, with respect to the importance of crystallization in the travertine domain.

More defined differences are highlighted among the volume distributions of calcite from lithogenic or anthropic source: in PM_{10} from travertine, the volume distribution of calcite shows a very narrowed shape, with maximum at 5 µm. Conversely, calcite of both road dust types shows broader distributions, extended to finer sizes, especially in the case of the volcanics-related road dust. In the latter, the curve is bi-modal with maxima at 3.8 and 1.8 µm, while in the travertine-related it is unimodal, with maximum at 5.3 µm similarly to calcite in travertine. The lithogenic or anthropic nature of processes tuning calcite size also influence the height of volume distributions of calcite.

In the first case, calcite particles mainly originate from crystals formed in the precipitation of calcium carbonate, as explained in Sect. 3.3; the variability of particle size is thus limited by chemical–physical conditions which rule travertine formation. In the second case, the variety of mechanical solicitations affecting the surface of paved roads, e.g. abrasion by vehicle riding, is described by a wider particle size range.

Discrepancies observed within volume distribution curves of Fig. 4 suggest also that individual particle densities may differ within the same silicate species or within calcite from different dust sources. It is acknowledged that the density of mineral particles may range significantly due to the petrological conditions (chemistry, kinetics and thermody-

ACPD
15, 13347–13393, 2015

namics involved in the crystallization process) associated to the different crystallization phases, by which mineral particles are formed.

In addition, some general considerations can be given on the particle density, by taking into account the distribution of particle mass percentage (discussed in Sect. 3.4.1) and ESD, with respect to the below/above 2 µm size threshold (coherently with the clay/non-clay distribution). Decreasing particle density should be expected from first to last of the following cases: (1) both mass percentage and ESD of particles mainly distributed below 2 µm; (2) mass percentage mainly observed below the 2 µm size and ESD comparably distributed with respect to this threshold; (3) both mass percentage and ESD mainly distributed in the size fraction above 2 µm. In Fig. 4, first case can be related to the calcite of road dust volcanics-related (80 % of particles showing ESD < 2 µm), while second case applies to quartz and kaolinite, and last case to feldspars and travertine calcite (60 and 80 %, respectively, of particles showing ESD > 2 µm).

Height differences among volume distributions of the dust types can be thus explained in connection with the different presence of a given mineral species in a dust type. In particular, while the content of kaolinite is higher in the volcanics than in siliciclastic dust, feldspars and quartz are more abundant in the latter. It is thus possible that these minerals play contrasting roles in defining the average particle density of siliciclastic dust, and consequently its volume distribution.

3.5 Microphysical, optical and radiative properties of the volcanics and travertine PM_{10} dust in the Rome area

3.5.1 Microphysical properties

In Fig. 5 results are showed of the fitting procedure applied to volcanics and travertine size distribution to obtain dust-specific log-normal curves.

The curves are reported with respect to the particle physical radius, as required by the 6SV radiative transfer code. The computed "chi squared" (χ^2) of fitting are respec-

ACPD
15, 13347–13393, 2015

tively 0.34 for volcanics and 0.59 for travertine. Considering twelve degrees of freedom corresponding to 13 size bins of the optical particle counter, both fitting are below the level of significance of 99.5 %. It is thus possible to refuse the null hypothesis that these curves cannot be fitted to a log-normal function. The following r_m and σ values of the volcanics and travertine size distributions are used thus, as input parameters of the Log-normal function (Eq. 1):

$$r_m^{volc} = 0.380, \quad \sigma^{volc} = 2.470; \quad r_m^{trav} = 1.220, \quad \sigma^{trav} = 1.650.$$

The other microphysical property required for 6SV run is the refractive index. In Fig. 6 the real (n) and imaginary (k) part of the refractive index have been interpolated at the 6SV twenty wavelengths (350; 400; 412; 443; 470; 488; 515; 550; 590; 633; 670; 694; 760; 860; 1240; 1536; 1650; 1950; 2250; 3750 nm), following the spectral data of water-insoluble (Kokhanovsky, 2008; WCP-112, 1986) and calcite-rich dust (Ghosh, 1999) refractive index, respectively related to volcanics and travertine. While the spectral trend of volcanics refractive index follows the commonly adopted trend used in the radiative transfer modelling (RTM) of the dust component (Kokhanovsky, 2008), the travertine dust, being mainly composed of calcite, is a non-absorbing aerosol, as the imaginary part of calcite refractive index is zero (Ghosh, 1999).

3.5.2 Optical properties

Optical properties of the volcanics and travertine contribution to Rome local mineral dust have been modeled in the twenty wavelengths of the 6SV code. In Fig. 7 the single-scattering albedo (SSA) and the asymmetry parameter (g) are shown, which are critical to analyze the aerosol-induced at-ground radiative flux (Kassianov et al., 2007). The lower SSA of volcanics, with respect to travertine, attests that the volcanics dust absorbs the solar radiation in the VISible (VIS) spectral domain, as commonly expected for mineral dust. Conversely, the SSA of travertine indicates that this dust type is a non-absorbing particulate. In Fig. 7b the spectral dependence of the asymmetry parameter (g) is showed for the volcanics and the travertine. As g is higher in the volcanics, in this

ACPD
15, 13347–13393, 2015

dust type particles show higher forward scattering than in the travertine, mainly in the Near-InfraRed (NIR) spectral domain. These findings suggest that the local geological dust of the Rome area affects both the VIS and NIR spectral domains; consequently an influence on the radiative field is expected as well.

3.5.3 Downward radiative flux at Bottom Of Atmosphere (BOA)

The radiative modeling has been focused on the downward component of the radiative impact at BOA due to the volcanics and travertine dust in Rome area. This part of the study represents a preliminary investigation of the direct radiative effect of the local dust component on the solar radiation at ground. In Fig. 8a the influence of both local dust types to the downward BOA solar irradiance (*I*) in the VIS and NIR spectral domain is shown. In order to evaluate the spectral dependence of the irradiance on the mineralogical composition of dust, the volcanics/travertine ratio is reported in Fig. 8b. In the VIS domain, the irradiance seems not to be affected by the mineralogical composition, as the BOA downward irradiance trends of two dust types almost overlap. However, in the NIR a sharp discrimination between the radiative impact of the volcanics and that of the travertine dust is revealed. Finally, the BOA downward flux obtained by integrating the downward solar irradiance over the solar spectral domain (250–4000 nm) is reported in Fig. 9. Both volcanic and travertine dusts leave the direct component unchanged, while the diffuse component depends strongly on the mineral composition. The scattered radiation of an atmosphere rich in travertine dust shows an higher diffuse component than in the case when a volcanics-rich atmosphere is considered. As a matter of fact, in the Rome site the total BOA downward flux is greater for an atmosphere where the only dust component is the travertine dust with respect to the sole presence of volcanic dust. These results need to be confirmed by a more in-depth analysis on the influence of the local geological dust re-suspended from topsoil on the Earth–atmosphere radiative balance, in Rome area. Nevertheless, the charge of differences existing in the Rome local mineral dust composition on the variability of

ACPD
15, 13347–13393, 2015

optical and radiative properties of the airborne aerosol appears as a key issue, to be further considered in the radiative balance analysis.

4 Conclusions

In this work, a knowledge gap was faced, which concerns how, and to which extent, the mineral dust locally re-suspended from rocks outcropped in a site/area may influence the composition of airborne aerosol, the direct interaction (light scattering and absorption) of the aerosol with solar radiation, and the radiative flux at BOA (Bottom Of Atmosphere), within the same source area of dust. To this goal, a methodology was developed, which is suitable for general application; nevertheless, results reported here are intrinsically narrowed to the features of Rome area. Investigation was carried following three paths: site-specific analysis of the geochemical and mineralogical environment, individual-particle based instrumental analysis aimed at determining the mineralogical and microphysical properties of dust, and modelling of the dust radiative effects with respect to optical features.

Main results concern relationships found between: (1) geochemical processes acting on the source rocks and mineral species associated to particles in the re-suspended PM_{10} fraction of different local dust types; (2) mineral composition of the PM_{10} dust and variability of dust microphysical properties (refractive index and size distribution); (3) dust-specific optical properties (single-scattering albedo and asymmetry parameter) of the PM_{10} fraction, and total downward flux at BOA in the VISible and Near Infrared (NIR) spectral domains.

First issue was discussed on all major outcropped domains in the Rome area (volcanic rocks, siliciclastic rocks, limestones, marlstones and travertine), and on the distinction between calcite from lithogenic source and calcite from paved road dust, while second and third issues focused on the compositional end-member of local dust types (volcanics and travertine).

ACPD
15, 13347–13393, 2015

With the exception of pure calcite (associated to PM_{10} from the travertine domain (Tivoli basin), and from road dust), PM_{10} dust types of the studied area show silicate-prevalent or calcite-prevalent compositions, depending on the outcropped source rocks: volcanics or siliciclastics in the first case, marlstones or limestones in the second case.

Rock weathering processes tune the size and mineral identity of PM_{10} particles in the silicate-prevalent dust types, more than other processes (e.g. debris formation, crystallization). On the other side, chemical precipitation of $CaCO_3$ influences mainly the particle composition of calcite-prevalent dust types. These differences reflect in the volume distributions, either of individual mineral species (kaolinite, quartz, feldspars, calcite), or of dust types.

Weathering processes can be related to larger size variability observed for some mineral species (e.g. kaolinite and quartz), with respect to feldspars and to lithogenic calcite.

In the lithogenic PM_{10} of Rome area, these minerals are instead mainly associated to crystallization or to $CaCO_3$ precipitation, occurring under defined chemical, kinetic and thermodynamic conditions which limit particle size and result in narrow volume distribution. Differences observed between calcite from lithogenic source and calcite from road dust suggest a major role of the variability of mechanical solicitations from vehicular riding on the particle size of road dust calcite. Volume distribution of the latter interestingly shows bimodal shape, broader width and larger contribution to fine fraction, differing significantly from lithogenic calcite and from other investigated mineral species.

These findings indicate that the microphysical properties of different crustal components (e.g. road dust, dust from building activities, transported mineral dust, etc.) may differ consistently with source type; optical properties are reasonably expected to differ consequently.

Spectral trends of the complex refractive index related to volcanics and travertine PM_{10}, in the VIS and NIR domains, show that travertine PM_{10} is a non-absorbing dust,

ACPD
15, 13347–13393, 2015

opposite to volcanics PM_{10}. We showed that these differences influence the diffuse component of BOA downward flux, which is higher in the simulated case of a travertine-rich atmosphere, coherently with the non-absorbing behavior of this dust type.

Finally, it is important to underline that above results could be assessed only by considering the entire solar spectral domain, instead of limiting the investigation to the VIS region.

Further research on these issues is needed, thus, as it may aid improving knowledge on the local effects of the presence of different crustal (natural or anthropic) components of aerosol at a specific site/area, in terms of aerosol interaction with solar radiation and radiative effects at BOA.

The Supplement related to this article is available online at doi:10.5194/acpd-15-13347-2015-supplement.

Acknowledgements. Thanks are due to Sergio Lo Mastro (Roma Tre University, Department of Geology, Rome, Italy), for X-ray diffraction analysis of the dust samples of this study. The authors are also grateful to Andrea Valdrè (FEI Company, USA), for his valuable scientific and technical advice with SEM XEDS microanalysis.

References

Armstrong, J. T. and Buseck, P. R.: Quantitative chemical analysis of individual microparticles using the electron microprobe: theoretical, Anal. Chem., 47, 2178–2192, 1975.

Bassani, C., Cavalli, R. M., and Pignatti, S.: Aerosol optical retrieval and surface reflectance from airborne remote sensing data over land, Sensors, 10, 6421–6438, doi:10.3390/s100706421, 2010.

Bassani, C., Cavalli, R. M., and Antonelli, P.: Influence of aerosol and surface reflectance variability on hyperspectral observed radiance, Atmos. Meas. Tech., 5, 1193–1203, doi:10.5194/amt-5-1193-2012, 2012.

ACPD
15, 13347–13393, 2015

Bergstrom, R. W., Russell, P. B., and Hignett, P.: Wavelength dependence of the absorption of black carbon particles: predictions and results from the TARFOX experiment and implications for the aerosol single scattering albedo, J. Atmos. Sci., 59, 567–577, 2002.
Bevington, P. R. and Robinson, D. K.: Data Reduction and Error Analysis for the Physical Sciences, 2nd edn., McGraw-Hill, New York, 1992.
Buseck, P. R. and Pósfai, M.: Airborne minerals and related aerosol particles: effects on climate and the environment, Colloquium Paper, P. Natl. Acad. Sci. USA, 96, 3372–3379, 1999.
Caquineau, S., Gaudichet, A., Gomes, L., and Legrand, M.: Mineralogy of Saharan dust transported over northwestern tropical Atlantic Ocean in relation to source regions, J. Geophys. Res., 107, 4251, doi:10.1029/2000JD000247, 2002.
Castaing, R.: Application des sondes électroniques à une méthode d'analyse ponctuelle chimique et cristallographique: publication ONERA (Office national d'études et de recherches aéronautiques/Institute for Aeronautical Research) N. 55, PhD thesis, University of Paris, Paris, 1952.
Choobari, O. A., Zawar-Reza, P., and Sturman, A.: The global distribution of mineral dust and its impacts on the climate system: a review, Atmos. Res., 138, 152–165, 2014.
Chožl, M., Deboudt, K., Osán, J., Flament, P., and Van Grieken, R.: Quantitative determination of low-Z elements in single atmospheric particles on boron substrates by automated scanning electron microscopy-energy-dispersive X-ray spectrometry, Anal. Chem., 77, 5686–5692, 2005.
Chožl, M., Deboudt, K., and Flament, P.: Evaluation of quantitative procedures for X-ray microanalysis of environmental particles, Microsc. Res. Techniq., 70, 996–1002, doi:10.1002/jemt.20510, 2007.
Claquin, T., Schulz, M., and Balkanski, Y. J.: Modeling the mineralogy of atmospheric dust sources, J. Geophys. Res., 104, 22243–22256, 1999.
Cosentino, D., Cipollari, P., Di Bella, L., Esposito, A., Faranda, F., Giordano, G., Gliozzi, E., Mattei, M., Mazzini, I., Porreca, M., and Funiciello, R.: Tectonics, sea level changes and palaeoenvironments in the early Pleistocene of Rome (Italy), Quaternary Res., 72, 143–155, 2009.
Costantini, E. A. C., Urbano, F., Aramini, G., Barbetti, R., Bellino, F., Bocci, M., Bonati, G., Fais, A., L'Abate, G., Loj, G., Magini, S., Napoli, R., Nino, P., Paolanti, M., Perciabosco, M., and Tascone, F.: Rationale and methods for compiling an atlas of desertification in Italy, Land Degrad. Dev., 20, 261–276, doi:10.1002/ldr.908, 2009.

ACPD
15, 13347–13393, 2015

D'Almeida, G. A.: On the variability of desert aerosol radiative characteristics, J. Geophys. Res., 92, 3017–3026, 1987.
D'Almeida, G. A., Koepke, P., and Shettle, E. P.: Atmospheric Aerosols, Global Climatology and Radiative Characteristics, A. Deepak Publishing, Hampton, VA, 1991.
Davies, C. N.: Size distribution of atmospheric particles, Aerosol Sci., 5, 293–300, 1974.
Di Biagio, C., Boucher, H., Caquineau, S., Chevaillier, S., Cuesta, J., and Formenti, P.: Variability of the infrared complex refractive index of African mineral dust: experimental estimation and implications for radiative transfer and satellite remote sensing, Atmos. Chem. Phys., 14, 11093–11116, doi:10.5194/acp-14-11093-2014, 2014.
Downs, R. T: The RRUFF Project: an Integrated Study of the Chemistry, Crystallography, Raman and Infrared Spectroscopy of Minerals, in: 19th General Meeting of the International Mineralogical Association in Kobe, Japan, 23 July–28, O03-13, 2006.
Dubovik, O. and King, M. D.: A flexible inversion algorithm for retrieval of aerosol optical properties from Sun and sky radiance measurements, J. Geophys. Res., 105, 20673–20696, 2000.
Dubovik, O., Holben, B., Eck, T. F., Smirnov, A., Kaufman, Y. J., King, M. D., Tanré, D., and Slutsker, I.: Variability of absorption and optical properties of key aerosol types observed in worldwide locations, J. Atmos. Sci., 59, 590–608, 2002.
Dürr, H. H., Meybeck, M., and Dürr, S. H.: Lithologic composition of the Earth's continental surfaces derived from a new digital map emphasizing riverine material transfer, Global Biogeochem. Cy., 19, GB4S10, doi:10.1029/2005GB002515, 2005.
Evans, R. D., Jefferson, I. F., Kumar, R., Hara-Dhand, K. O., and Smalley, I. J.: The nature and early history of airborne dust from north Africa in particular the Lake Chad Basin, J. Afr. Earth Sci., 39, 81–87, 2004.
Faccenna, C., Funiciello, R., and Soligo, M.: Origin and deposition of the Lapis Tiburtinus travertine, in: The Colli Albani Volcano, edited by: Funiciello, R. and Giordano, G., The Geological Society for IAVCEI, Bath, United Kingdom, 215–228, ISBN: 978-1-86239-307-3, 2010.
Falkovich, A. H., Ganor, E., Levin, Z., Formenti, P., and Rudich, Y.: Chemical and mineralogical analysis of individual mineral dust particles, J. Geophys. Res., 106, 18029–18036, 2001.
Fletcher, R. A., Ritchie, N. W. M., Anderson, I. M., and Small, J. A.: Microscopy and microanalysis of individual collected particles, in: Aerosol Measurement: Principles, Techniques, and Applications, 3rd edn., edited by: Kulkarni, P., Baron, P. A., and Willeke, K., John Wiley & Sons Ltd, Hoboken, New Jersey, USA, chapt. 10, 195–198, 2011.

ACPD
15, 13347–13393, 2015

Formenti, P., Caquineau, S., Desboeufs, K., Klaver, A., Chevaillier, S., Journet, E., and Rajot, J. L.: Mapping the physico-chemical properties of mineral dust in western Africa: mineralogical composition, Atmos. Chem. Phys., 14, 10663–10686, doi:10.5194/acp-14-10663-2014, 2014.

Geoportale Nazionale: available at: http://www.pcn.minambiente.it (last access: 20 October 2014), Ministero dell'Ambiente e della Tutela del Territorio e del Mare, Rome, Italy, 2011.

Ghosh, G.: Dispersion-equation coefficients for the refractive index and birefringence of calcite and quartz crystals, Opt. Commun., 163, 95–102, doi:10.1016/S0030-4018(99)00091-7, 1999.

Giampaolo, C. and Lo Mastro, S.: Analisi (semi)quantitativa delle argille mediante diffrazione a raggi X, in: Incontri Scientifici, Vol. II, edited by: Fiore, S., C. N. R. Istituto di Ricerca sulle Argille, Tito Scalo (PZ), Italy, 109–146, 2000.

Goldstein, J. I., Williams, D. B., and Cliff, G.: Quantitative X-ray analysis, in: Principles of Analytical Electron Microscopy, chapt. 5, edited by: Joy, D. C., Romig Jr., A. D., and Goldstein, J. I., Springer, New York, USA, ISBN: 978-1-4899-2039-3, 1986.

Hansell Jr., R. A., Reid, J. S., Tsay, S. C., Roush, T. L., and Kalashnikova, O. V.: A sensitivity study on the effects of particle chemistry, asphericity and size on the mass extinction efficiency of mineral dust in the earth's atmosphere: from the near to thermal IR, Atmos. Chem. Phys., 11, 1527–1547, doi:10.5194/acp-11-1527-2011, 2011.

Hsu, Y. and Divita, F.: SPECIATE 4.2, Speciation Database Development Documentation, Final Report, EPA/600-R-09/-38, United States Environmental Protection Agency, USA, 2009.

Jackson, M., Deocampo, D., Marra, F., and Scheetz, B.: Mid-Pleistocene Pozzolanic volcanic ash in ancient Roman concretes, Geoarchaeology, 25, 36–74, 2010.

Jeong, G. Y.: Bulk and single-particle mineralogy of Asian dust and a comparison with its source soils, J. Geophys. Res., 113, D02208, doi:10.1029/2007jd008606, 2008.

Journet, E., Balkanski, Y., and Harrison, S. P.: A new data set of soil mineralogy for dust-cycle modeling, Atmos. Chem. Phys., 14, 3801–3816, doi:10.5194/acp-14-3801-2014, 2014.

Kalashnikova, O. V. and Sokolik, I. N.: Importance of shapes and compositions of wind-blown dust particles for remote sensing at solar wavelengths, Geophys. Res. Lett., 29, 1398, doi:10.1029/2002GL014947, 2002.

Kalashnikova, O. V. and Sokolik, I. N.: Modeling the radiative properties of non-spherical soil-derived mineral aerosols, J. Quant. Spectrosc. Ra., 87, 137–166, 2004.

ACPD
15, 13347–13393, 2015

Kandler, K., Benker, N., Bundke, U., Cuevas, E., Ebert, M., Knippertz, P., Rodríguez, S., Schütz, L., and Weinbruch, S.: Chemical composition and complex refractive index of Saharan mineral dust at Izaña, Tenerife (Spain) derived by electron microscopy, Atmos. Environ. , 41, 8058–8074, 2007.

Kandler, K., Schütz, L., Deutscher, C., Ebert, M., Hofmann, H., Jäckel, S., Jaenicke, R., Knippertz, P., Lieke, K., Massling, A., Petzold, A., Schladitz, A., Weinzierl, B., Wiedensohler, A., Zorn, S., and Weinbruch, S.: Size distribution, mass concentration, chemical and mineralogical composition and derived optical parameters of the boundary layer aerosol at Tinfou, Morocco, during SAMUM 2006, Tellus B, 61, 32–50, 2009.

Karner, D. B., Marra, F., and Renne, P. R.: The history of the Monti Sabatini and Alban Hills volcanoes: groundwork for assessing volcanic-tectonic hazards for Rome, J. Volcanol. Geoth. Res., 107, 185–219, 2001.

Kassianov, E. I., Flynn, C. J., Ackerman, T. P., and Barnard, J. C.: Aerosol single-scattering albedo and asymmetry parameter from MFRSR observations during the ARM Aerosol IOP 2003, Atmos. Chem. Phys., 7, 3341–3351, doi:10.5194/acp-7-3341-2007, 2007.

Kaufman, Y. J., Tanre, D., Gordon, H. R., Nakajima, T., Lenoble, J., Frouin, R., Grassl, H., Herman, B. M., King, M. D., and Teillet, P. M.: Passive remote sensing of tropospheric aerosol and atmospheric correction for the aerosol effect, J. Geophys. Res., 102, 16815–16830, 1997.

Kim, H. K., Hwang, H. J., and Un Ro, C.: Single-particle characterization of soil samples collected at various arid areas of China, using low-Z particle electron probe X-ray microanalysis, Spectrochim. Acta B, 61, 393–399, 2006.

Kokhanovsky, A. A.: Aerosol Optics. Light Absorption and Scattering by Particles in the Atmosphere, Springer-Praxis, Chichester, United Kingdom, ISBN 978-3-540-23734-1, 2008.

Kotchenova, S. Y., Vermote, E. F., and Levy, R., and Lyapustin, A.: Radiative transfer codes for atmospheric correction and aerosol retrieval: intercomparison study, Appl. Optics, 47, 2215–2226, doi:10.1364/AO.47.002215, 2008.

Krueger, B. J., Grassian, V. H., Cowin, J. P., and Laskin, A.: Heterogeneous chemistry of individual mineral dust particles from different dust source regions: the importance of particle mineralogy, Atmos. Environ. , 38, 6253–6261, 2004.

Kulkarni, P., Baron, P. A., and Willeke, K.: Fundamentals of single particle transport, in: Aerosol Measurement: Principles, Techniques, and Applications, 3rd edn., edited by: Kulkarni, P.,

ACPD
15, 13347–13393, 2015

Baron, P. A., and Willeke, K., John Wiley & Sons Ltd., Hoboken, New Jersey, USA, chapt. 8, 24–25, 2011.
Levin, Z., Ganor, E., and Gladstein, V.: The effects of desert particles coated with sulfate on rain formation in the eastern Mediterranean, J. Appl. Meteorol., 35, 1511–1523, 1996.
Mahowald, N., Albani, S., Kok, J. F., Engelstaeder, S., Scanza, R., Ward, D. S., and Flanner, M. G.: The size distribution of desert dust aerosols and its impact on the Earth system, Aeolian Res., 15, 53–71, 2014.
Meloni, D., di Sarra, A., Pace, G., and Monteleone, F.: Aerosol optical properties at Lampedusa (Central Mediterranean). 2. Determination of single scattering albedo at two wavelengths for different aerosol types, Atmos. Chem. Phys., 6, 715–727, doi:10.5194/acp-6-715-2006, 2006.
Moore, D. M. and Reynolds, R. C.: X-ray Diffraction and the Identification and Analysis of Clay Minerals, Oxford University Press, Oxford, 1997.
Moreno, T., Amato, F., Querol, X., Alastuey, A., Elvira, J., and Gibbons, W.: Bedrock controls on the mineralogy and chemistry of PM_{10} extracted from Australian desert sediments, Environ. Geol., 57, 411–420, doi:10.1007/s00254-008-1312-2, 2009.
Müller, T., Schladitz, A., Massling, A., Kaaden, N., Kandler, K., and Wiedensohler, A.: Spectral absorption coefficients and imaginary parts of refractive indices of Saharan dust during SAMUM-1, Tellus B, 61, 79–95, 2009.
Nash, J. C.: Compact Numerical Methods for Computers: Linear Algebra and Function Minimisation, 2nd edn., Adam Hilger, Bristol, 1990.
Newbury, D. E. and Ritchie, N. W. M.: Is scanning Electron Microscopy/Energy Dispersive X-Ray Spectrometry (SEM/EDS) quantitative?, Scanning, 35, 141–168, 2013.
Nickovic, S., Vukovic, A., Vujadinovic, M., Djurdjevic, V., and Pejanovic, G.: Technical Note: High-resolution mineralogical database of dust-productive soils for atmospheric dust modeling, Atmos. Chem. Phys., 12, 845–855, doi:10.5194/acp-12-845-2012, 2012.
OAQPS Staff: Review of the National Ambient Air Quality Standards for Particulate Matter: Policy Assessment of Scientific and Technical Information, OAQPS Staff Paper, EPA-452/R-05-005, chapt. 2, United States Environmental Protection Agency, USA, 2005.
Papayannis, A., Mamouri, R. E., Amiridis, V., Remoundaki, E., Tsaknakis, G., Kokkalis, P., Veselovskii, I., Kolgotin, A., Nenes, A., and Fountoukis, C.: Optical-microphysical properties of Saharan dust aerosols and composition relationship using a multi-wavelength Raman

ACPD
15, 13347–13393, 2015

lidar, in situ sensors and modelling: a case study analysis, Atmos. Chem. Phys., 12, 4011–4032, doi:10.5194/acp-12-4011-2012, 2012.
Peng, F. and Effler, S. W.: Suspended minerogenic particles in a reservoir: light-scattering features from individual particle analysis, Limnol. Oceanogr., 52, 204–216, 2007.
Pentecost, A.: Travertine, Springerverlag, Berlin, Germany, chapt. 7, 124, ISBN: 1-4020-3523-3, 2005.
Perrino, C., Canepari, S., Catrambone, M., Dalla Torre, S., Rantica, E., and Sargolini, T.: Influence of natural events on the concentration and composition of atmospheric particulate matter, Atmos. Environ. , 43, 4766–4779, 2009.
Pietrodangelo, A., Salzano, R., Rantica, E., and Perrino, C.: Characterisation of the local topsoil contribution to airborne particulate matter in the area of Rome (Italy). Source profiles, Atmos. Environ. , 69, 1–14, 2013.
Potts, P. J.: A Handbook of Silicate Rock Analysis, Springer Science + Business Media, New York, USA, ISBN: 978-0-216-93209-8, 1992.
R Core Team: R: a Language and Environment for Statistical Computing, available at: http://www.R-project.org/ (last access: April 2014), R Foundation for Statistical Computing, Vienna, Austria, 2013.
Rashki, A., Eriksson, P. G., de W. Rautenbach, C. J., Kaskaoutis, D. G., Grote, W., and Dykstra, J.: Assessment of chemical and mineralogical characteristics of airborne dust in the Sistan region, Iran, Chemosphere, 90, 227–236, 2013.
Reid, J. S., Jonsson, H. H., Maring, H. B., Smirnov, A., Savoie, D. L., Cliff, S. S., Reid, E. A., Livingston, J. M., Meier, M. M., Dubovik, O., and Tsay, S. C.: Comparison of size and morphological measurements of coarse mode dust particles from Africa, J. Geophys. Res., 108, 8593, doi:10.1029/2002JD002485, 2003.
Rocha-Lima, A., Martins, J. V., Remer, L. A., Krotkov, N. A., Tabacniks, M. H., Ben-Ami, Y., and Artaxo, P.: Optical, microphysical and compositional properties of the Eyjafjallajökull volcanic ash, Atmos. Chem. Phys., 14, 10649–10661, doi:10.5194/acp-14-10649-2014, 2014.
Rudnick, R. L. and Gao, S.: Composition of the continental crust, in: Treatise on Geochemistry, vol. 3, edited by: Holland, H. D. and Turekian, K. K., Elsevier, Amsterdam, 1–64, ISBN: 978-0-08-043751-4, 2003.
Sarbas, B. and Nohl, U.: The GEOROC database as part of a growing geoinformatics network, in: Geoinformatics 2008 – Data to Knowledge, Proceedings, U.S. Geological Survey Scientific Investigations Report 2008-5172, available at: http://georoc.mpch-mainz.gwdg.de/

ACPD
15, 13347–13393, 2015

georoc/Start.asp (last access: October 2013), edited by: Brady, S. R., Sinha, A. K., and Gundersen, L. C., 42–43, 2008.
Scheuvens, D., Schütz, L., Kandler, K., Ebert, M., and Weinbruch, S.: Bulk composition of northern African dust and its source sediments – a compilation, Earth-Sci. Rev., 116, 170–194, 2013.
Simon, H., Beck, L., Bhave, P. V., Divita, F., Hsu, Y., Luecken, D., Mobley, J. D., Pouliot, G. A., Reff, A., Sarwar, G., and Strum, M.: The development and uses of EPA's SPECIATE database, Atmos. Pollut. Res., 1, 196–206, 2010.
Smith, A. J. A. and Grainger, R. G.: Does variation in mineral composition alter the short-wave light scattering properties of desert dust aerosol?, J. Quant. Spectrosc. Ra., 133, 235–243, 2014.
Sokolik, I. N. and Toon, O. B.: Incorporation of mineralogical composition into models of the radiative properties of mineral aerosol from UV to IR wavelengths, J. Geophys. Res., 104, D8, 9423–9444, 1999.
Sokolik, I. N., Winker, D. M., Bergametti, G., Gillette, A., Carmichael, G., Kaufman, Y. J., Gomes, L., Schuetz, L., and Penner, J. E.: Introduction to special Sect.: Outstanding problems in quantifying the radiative impacts of mineral dust, J. Geophys. Res., 107, 18015–18027, 2001.
Stuut, J.-B., Smalley, I., and O'Hara-Dhand, K.: Aeolian dust in Europe: African sources and European deposits, Quatern. Int., 198, 234–245, 2009.
Van Dyck, P., Storms, H., and Van Grieken, R.: Automated quantitative electron microprobe analysis of particulate material, J. Phys.-Paris, C2, suppl. 2, 781–784, doi:10.1051/jphyscol:19842179, 1984.
Vermote, E. F., Tanrè, D., Deuzè, J. L., Herman, M., and Morcrette, J. J.: Second simulation of the satellite signal in the solar spectrum, 6S: an overview, IEEE T. Geosci. Remote, 35, 675–686, doi:10.1109/36.581987, 1997.
Vermote, E. F., Tanrè, D., Deuzè, Herman, M., Morcrette, J. J., and Kotchenova, S. Y.: Second Simulation of a Satellite Signal in the Solar Spectrum – Vector (6SV), 6S User Guide Version 3, available at: http://6s.ltdri.org (last access: April 2014), National Aeronautics and Space Administration, USA, 2006.
Viana, M., Pey, J., Querol, X., Alastuey, A., de Leeuw, F., and Lükewille, A.: Natural sources of atmospheric aerosols influencing air quality across Europe, Sci. Total. Environ., 472, 825–833, 2014.

ACPD
15, 13347–13393, 2015

Wagner, R., Ajtai, T., Kandler, K., Lieke, K., Linke, C., Müller, T., Schnaiter, M., and Vragel, M.: Complex refractive indices of Saharan dust samples at visible and near UV wavelengths: a laboratory study, Atmos. Chem. Phys., 12, 2491–2512, doi:10.5194/acp-12-2491-2012, 2012.

WCP-112: A Preliminary Cloudless Standard Atmosphere for Radiation Computation, World Meteorological Organization, Geneva, 1986.

White, A. F. and Buss, H. L.: Natural weathering rates of silicate minerals, in: Treatise on Geochemistry, 2nd edn., vol. 7, edited by: Holland, H. D. and Turekian, K. K., Elsevier, Amsterdam, ISBN: 978-0-08-043751-4, 115–155, 2014.

Wilks, D. S.: Statistical Methods in the Atmospheric Sciences, 2nd edn., Elsevier, Amsterdam, chapt. 5, ISBN: 13:978-0-12-751966-1, 2006.

Ziebold, T. O.: Precision and sensitivity in electron microprobe analysis, Anal. Chem., 39, 858–861, 1967.

ACPD
15, 13347–13393, 2015

Table 1. Quality assessment of SEM XEDS microanalysis. %Δ are reported as absolute values.

	Dust	Mineral particle	K	Na	Ca	Mg	Fe	Mn	Al	Si	Ti
Repeatability (% rsd)	Volcanics		10	28	14	19	12	39	6	6	29
	Road dust		35	43	33	23	33	34	36	31	54
	Siliciclastics		15	24	10	13	17	31	11	8	56
	Travertine		17	25	2	25	21	31	14	6	54
Consistency with XRF (% Δ[a] ± prop. error)	Volcanics		2.4 ± 0.1	55.4 ± 0.1	22.7 ± 0.3	–	32.2 ± 0.1	500 ± 10	15.8 ± 0.2	10.8 ± 0.1	41.4 ± 0.5
	Road dust		37.5 ± 0.3	> 100	28.2 ± 0.1	> 100	37.7 ± 0.7	> 100	22.3 ± 0.2	37.4 ± 0.2	87.6 ± 1.4
	Siliciclastics		22.2 ± 0.1	78.7 ± 2.1	39.2 ± 0.7	52.4 ± 0.3	10.8 ± 0.2	470 ± 10	2.8 ± 0.1	50.7 ± 0.2	7.8 ± 0.5
Accuracy ($g\,cm^{-3}$)		Quartz	–	–	–	–	–	–	–	3.4 ± 0.02	–
		Kaersutite	0.07 ± 0.02	0.04 ± 0.03	0.24 ± 0.02	0.23 ± 0.03	0.67 ± 0.01	0.02 ± 0.01	0.49 ± 0.02	1.12 ± 0.02	0.11 ± 0.02
		Calcite	–	–	4.1 ± 0.02	–	–	–	–	–	–
Accuracy (% Δ[b] ± prop. error)		Quartz	–	–	–	–	–	–	–	28 ± 0.4	–
		Kaersutite	37.3 ± 0.6	94.1 ± 18.3	47.4 ± 1.5	38.6 ± 0.3	28.6 ± 0.2	61.5 ± 1.8	28 ± 0.3	6.4 ± 0.3	40 ± 2
		Calcite	–	–	52 ± 1	–	–	–	–	–	–

[a] Reference term of %Δ: bulk elemental composition of local dust by ED-XRF (Pietrodangelo et al., 2013).
[b] Reference term of %Δ: bulk elemental composition of standard mineral (EDAX Inc.).

ACPD
15, 13347–13393, 2015

Table 2. Average mineral composition (%wt) of dust samples by XRD analysis.

	Volcanic rocks	Siliciclastic rocks	Marlstones	Road dust (Volcanics)	Road dust (Travertine)	Travertine*
Phyllosilicates	57	52	26	7	–	–
Tectosilicates	18	6	0.7	8.7	6	–
Inosilicates	26	–	1.5	22.7	10.2	–
Quartz	4	11	4	1.3	3	–
Calcite	–	31	68	60.3	81	> 90

* After Pentecost (2005).

ACPD
15, 13347–13393, 2015

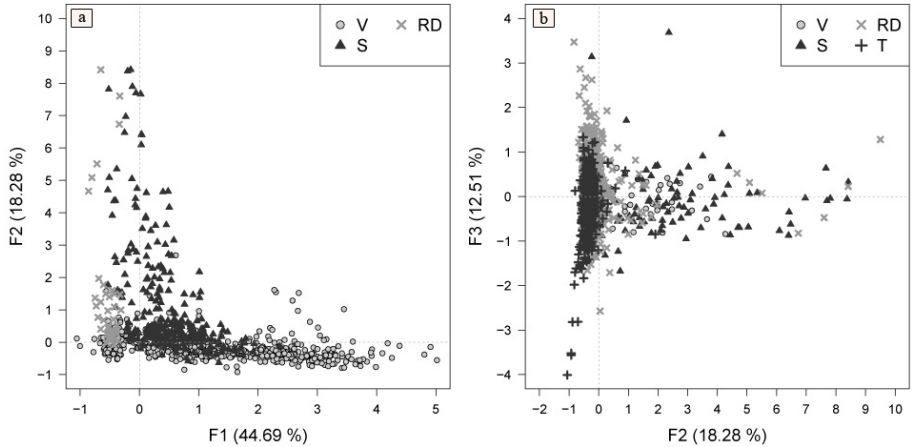

Figure 1. PCA of elemental ratios calculated on individual dust particles composition: score plots of factors (F1, F2, F3) with eigenvalue higher than unity. V: volcanics; S: siliciclastics; RD: road dust; T: travertine.

ACPD
15, 13347–13393, 2015

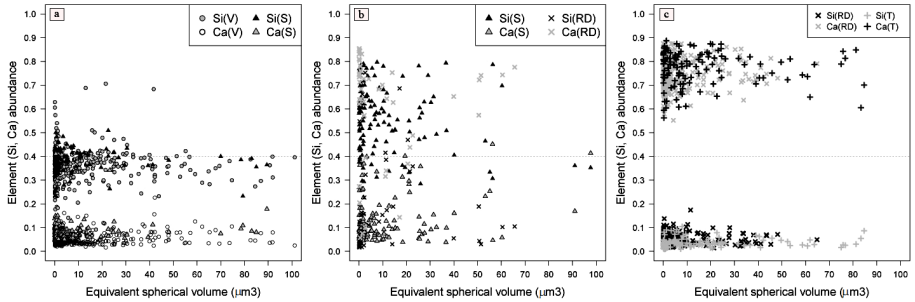

Figure 2. Ca and Si abundances of particles with highest PCA score in F1 **(a)**, F2 **(b)**, or F3 **(c)**, plotted vs. the particle equivalent spherical volume.

ACPD
15, 13347–13393, 2015

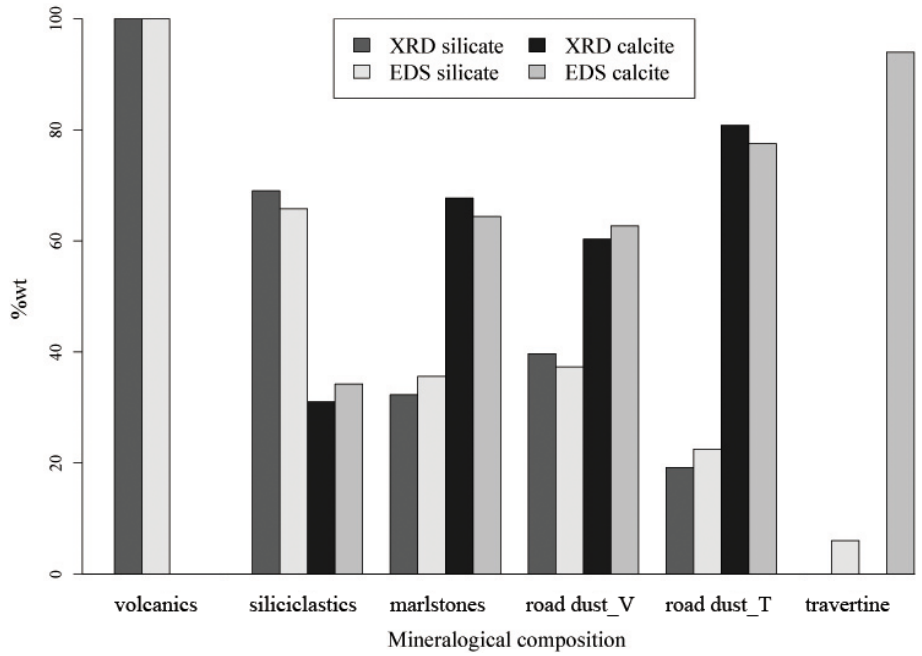

Figure 3. Total silicate (including quartz) and calcite amounts (%wt) of dust samples, obtained by X-ray diffraction bulk analysis and SEM XEDS particle microanalysis.

ACPD
15, 13347–13393, 2015

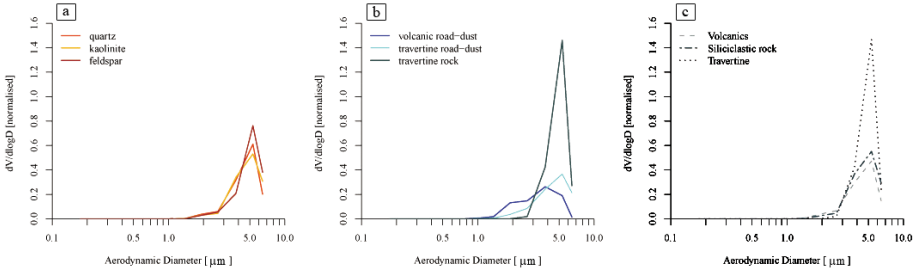

Figure 4. Normalised volume size distributions of most abundant silicates **(a)**, calcite **(b)**, and local dust types **(c)** in the PM_{10} fraction. Calcite is differentiated by natural (travertine) or anthropic (road dust) origin.

ACPD
15, 13347–13393, 2015

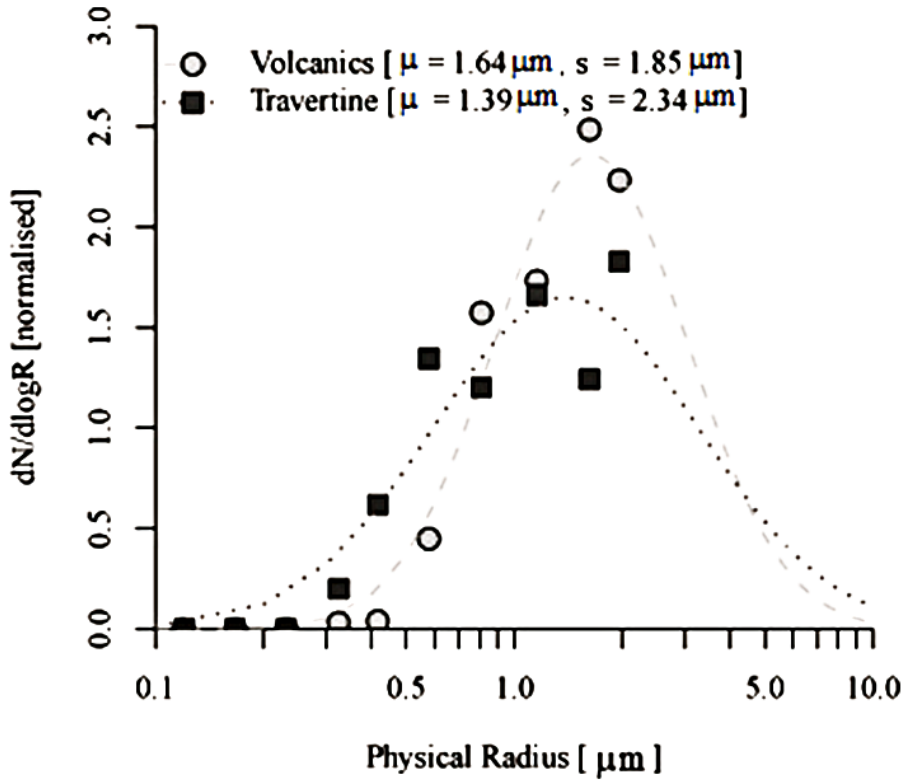

Figure 5. Probability density function fitted to log-normal distribution of the volcanics and travertine PM_{10} dust.

ACPD
15, 13347–13393, 2015

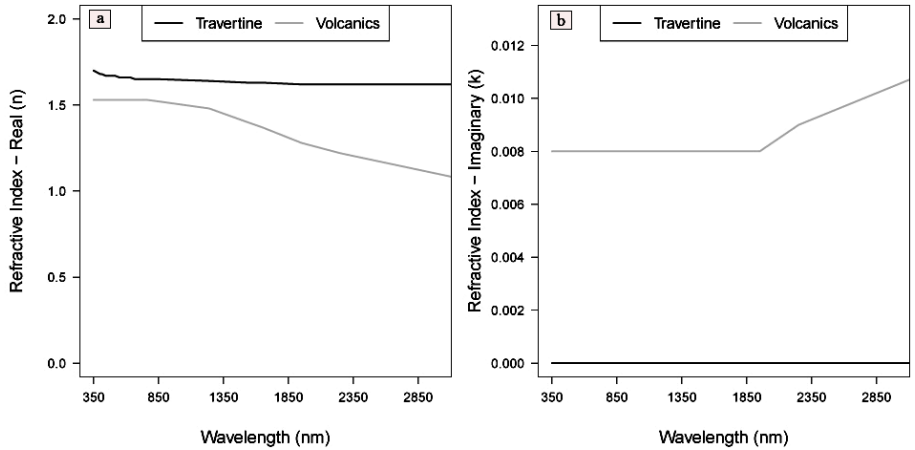

Figure 6. Real **(a)** and imaginary **(b)** part of refractive index of the volcanics and travertine PM_{10} dust.

ACPD
15, 13347–13393, 2015

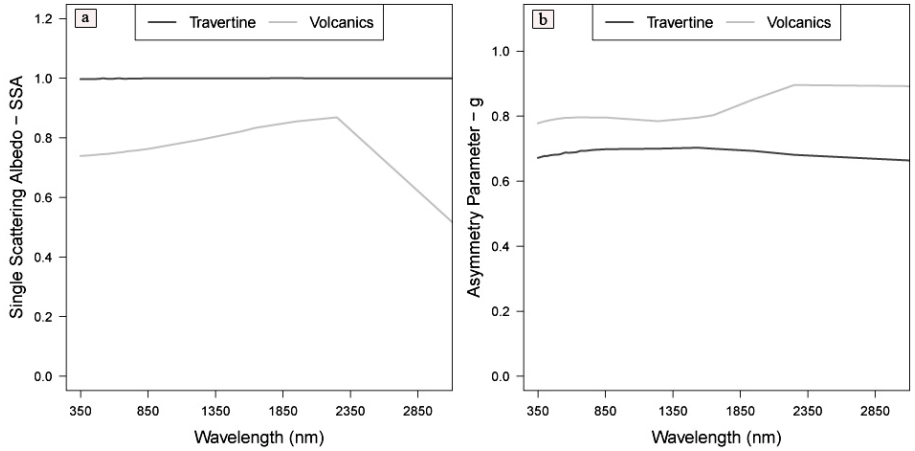

Figure 7. Single scattering albedo **(a)** and asymmetry parameter **(b)** of the volcanics and travertine PM_{10} dust.

ACPD
15, 13347–13393, 2015

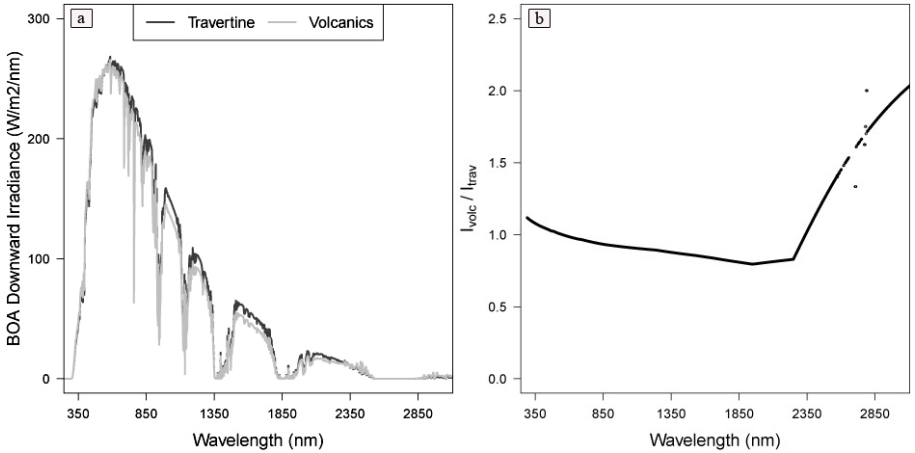

Figure 8. BOA downward solar irradiance **(a)** of an atmosphere composed by only volcanics, or travertine, PM_{10} dust, and volcanics to travertine irradiance ratio **(b)**.

ACPD
15, 13347–13393, 2015

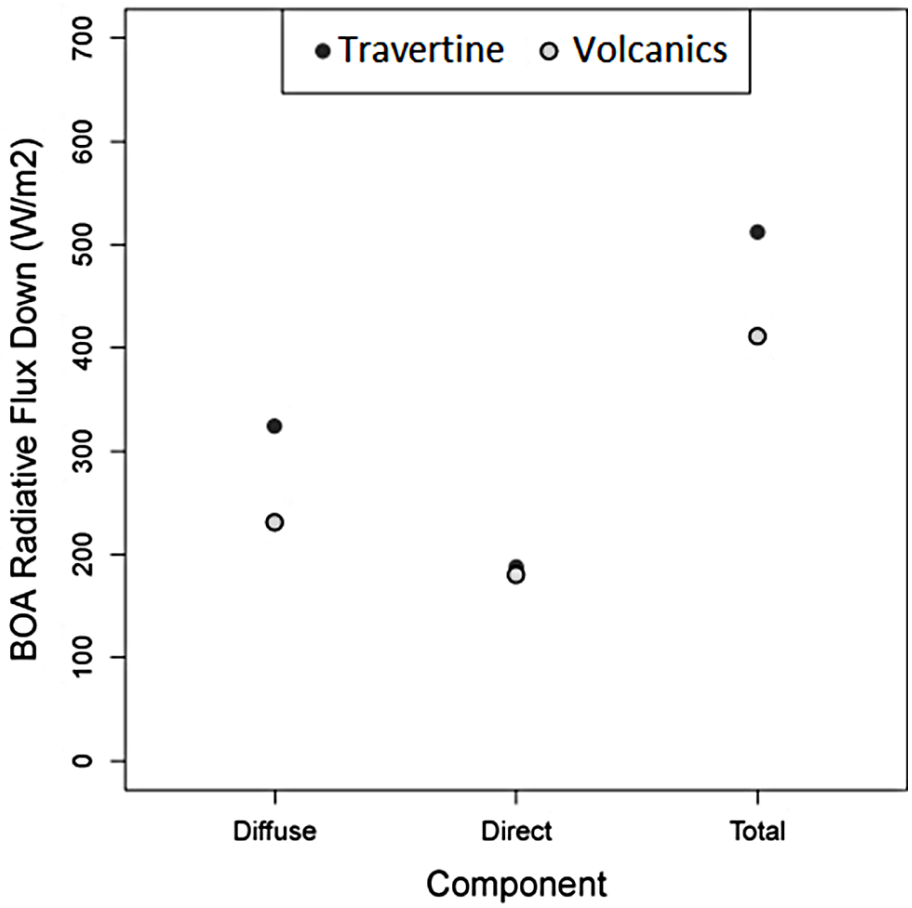

Figure 9. Diffuse, direct and total BOA downward radiative flux ($W m^{-2}$) over the 250–4000 nm spectral domain, simulated by the 6SV code.

ACPD
15, 13347–13393, 2015